Oxygen-coupled redox regulation of the skeletal muscle ryanodine receptor-Ca^{2+} release channel by NADPH oxidase 4

Qi-An Sun[a,b,c], Douglas T. Hess[a,b,c], Leonardo Nogueira[d], Sandro Yong[e], Dawn E. Bowles[f], Jerry Eu[d], Kenneth R. Laurita[e], Gerhard Meissner[g], and Jonathan S. Stamler[a,b,c,1]

[a]Institute for Transformative Molecular Medicine and [b]Department of Medicine, Case Western Reserve University, Cleveland, OH 44106; [c]University Hospitals, Cleveland, OH 44106; [d]Departments of Medicine and [f]Surgery, Duke University Medical Center, Durham, NC 27710; [e]Heart and Vascular Research Center, Case Western Reserve University, Cleveland, OH 44109; and [g]Department of Biochemistry and Biophysics, University of North Carolina, Chapel Hill, NC 27599

Edited* by Irwin Fridovich, Duke University Medical Center, Durham, NC, and approved August 9, 2011 (received for review June 13, 2011)

Physiological sensing of O_2 tension (partial O_2 pressure, pO_2) plays an important role in some mammalian cellular systems, but striated muscle generally is not considered to be among them. Here we describe a molecular mechanism in skeletal muscle that acutely couples changes in pO_2 to altered calcium release through the ryanodine receptor–Ca^{2+}-release channel (RyR1). Reactive oxygen species are generated in proportion to pO_2 by NADPH oxidase 4 (Nox4) in the sarcoplasmic reticulum, and the consequent oxidation of a small set of RyR1 cysteine thiols results in increased RyR1 activity and Ca^{2+} release in isolated sarcoplasmic reticulum and in cultured myofibers and enhanced contractility of intact muscle. Thus, Nox4 is an O_2 sensor in skeletal muscle, and O_2-coupled hydrogen peroxide production by Nox4 governs the redox state of regulatory RyR1 thiols and thereby governs muscle performance. These findings reveal a molecular mechanism for O_2-based signaling by an NADPH oxidase and demonstrate a physiological role for oxidative modification of RyR1.

redox signaling | oxygen sensing | S-nitrosylation

Specialized mammalian sensory cells transduce varying O_2 levels, but the mechanisms of O_2 sensing and O_2-based signaling have not been elucidated fully. In particular, reversible changes in ion channel activity often are implicated in physiological responses to O_2, but the molecular bases of these changes are unknown. We previously have described an O_2-sensing and -signaling mechanism in mammalian skeletal muscle that operates on the ryanodine receptor–Ca^{2+}-release channel (RyR1), the principal source of Ca^{2+} release from the sarcoplasmic reticulum (SR) (1, 2). At relatively low partial pressure of O_2 (pO_2), endogenously generated NO regulates RyR1 activity by S-nitrosylation of a single Cys thiol (1, 3). At higher pO_2, RyR1 activity is enhanced independently of NO in association with the oxidation of a separate, small set of Cys thiols (1). Oxidation of RyR1 thiols at high pO_2 and reduction following transition from high to low pO_2 are observed in isolated SR vesicles (1). However, the molecular mechanisms within the SR that mediate this O_2-based redox cycle have not been determined. Here we show that the redox enzyme NADPH oxidase 4 (Nox4) is a constituent of the SR and that hydrogen peroxide (H_2O_2) produced by Nox4 in proportion to pO_2 over a physiological range serves as an essential effector of pO_2-dependent regulation of RyR1 redox status and function. These data demonstrate physiological regulation by reactive oxygen species (ROS) of RyR1 and suggest insights into the molecular mechanisms of O_2 sensing and O_2-based signaling in mammalian cells.

Results

RyR1 activity in an SR-enriched subcellular fraction (SR vesicles) was enhanced progressively at pO_2 of 1% O_2, 5% O_2, and 20% O_2 (ambient pO_2) (Fig. 1*A*); these levels largely recapitulate the physiological muscle O_2 gradient and extend to oxidative stress (4–7). Production of ROS was enhanced similarly, as assessed by measuring fluorescence resulting from conversion of dihydroethidium (DHE) (8) (Fig. 1*B*) (or of 2′,7′-dichlorofluorescin; *vide infra*). The increase in RyR1 activity at high (20% O_2) versus low (1% O_2) pO_2 was largely eliminated by polyethylene glycol (PEG)-catalase (Fig. 1*C*). Thus, an endogenous SR mechanism generates ROS in a pO_2-dependent fashion that regulates RyR1 activity, and H_2O_2 is apparently the active species.

Potential sources of pO_2-coupled H_2O_2 production within the SR include mitochondria, which have been implicated in pO_2 sensing in multiple cell types (9–11), xanthine oxidase, which plays a role in ROS generation in cardiac muscle (12), and one or more forms of Nox (13, 14). However, in SR vesicles, enhancement of mitochondrial ROS production by antimycin A had no affect on RyR1 activity (Fig. S1), and inhibition of xanthine oxidase with allopurinol affected neither ROS production nor RyR1 activity (Fig. S2).

All forms of Nox catalyze electron transfer from NADPH to molecular oxygen to generate superoxide and thereby H_2O_2 or to generate H_2O_2 directly in the case of the dual oxidases (Duoxs) and perhaps Nox4 (13–15). In SR vesicles prepared from rabbit (Fig. 2 *A* and *B*) or mouse (Fig. S3 *A* and *B*) hind-limb skeletal muscle, addition of 1 mM NADPH resulted in substantial increases in both ROS production and RyR1 activity at high pO_2. Enhancement of both ROS production and RyR1 activity at high versus low pO_2 was largely eliminated by diphenyleneiodonium (DPI), a flavoprotein inhibitor well-characterized as an inhibitor of Nox (Fig. 2 *A* and *B* and Fig. S3 *A* and *B*), and by the recently described Nox inhibitor, 3-benzyl-7-(benzoxazolyl)thio-1,2,3-triazolo[4,5-d]pyrimidine (VAS2870) (Fig. S3 *C* and *D*) (16). Thus, the pO_2-coupled activity within the SR that regulates RyR1 through ROS production exhibits properties of a Nox. Note that ROS production by a Nox in SR vesicles in the absence of added NADPH would require endogenous dinucleotide. We determined that NADPH+NADP is present at 126 ± 12.8 pmol/mg protein and 98.3 ± 10.8 pmol/mg protein in SR vesicles isolated from mouse and rabbit muscle, respectively (n = 3); levels in whole mouse muscle homogenates were 785 ± 83.2 pmol/mg protein (n = 3) (NADP+/NADPH Quantification Kit; Biovision Research Products).

We then measured free thiols in RyR1 isolated from solubilized SR vesicles (1) after incubation at low or high pO_2. RyR1 at low pO_2 possessed about 40 free Cys thiols as assessed by mono-

Author contributions: Q.-A.S., D.T.H., K.R.L., G.M., and J.S.S. designed research; Q.-A.S., L.N., and S.Y. performed research; D.E.B. and J.E. contributed new reagents/analytic tools; Q.-A.S., D.T.H., and S.Y. analyzed data; and Q.-A.S., D.T.H. and J.S.S. wrote the paper.

The authors declare no conflict of interest.

*This Direct Submission article had a prearranged editor.

[1]To whom correspondence should be addressed. E-mail: jonathan.stamler@case.edu.

This article contains supporting information online at www.pnas.org/lookup/suppl/doi:10.1073/pnas.1109546108/-/DCSupplemental.

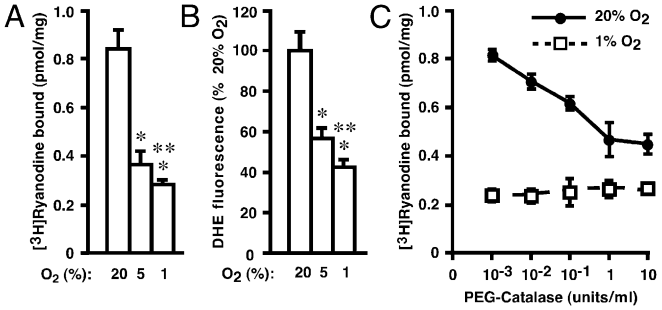

Fig. 1. pO_2-dependent regulation of RyR1 by endogenous ROS. (*A* and *B*) In SR vesicles isolated from rabbit hind-limb skeletal muscle, RyR1 activity assessed by [^{3}H]-ryanodine binding (*A*) and ROS production assessed by DHE fluorescence (*B*) were enhanced progressively as pO_2 increased from 1% to 5–20% O_2. Single and double asterisks indicate significant difference versus 20% O_2 and 5% O_2, respectively ($P < 0.01$; $n = 3$–5). (*C*) PEG-catalase largely eliminated the enhancement of RyR1 activity at high versus low pO_2 ($n = 3$).

bromobimane labeling, and a small set (5.4 thiols) was lost at high versus low pO_2 (39.9 ± 2.8 free thiols at low pO_2 versus 34.5 ± 2.4 free thiols at high pO_2) (Table 1). DPI and PEG-catalase had no apparent effect on free thiol number at low pO_2 (Table 1). However, thiol loss at high versus low pO_2 was largely prevented by both DPI (39.6 ± 1.2 free thiols at low pO_2 versus 38.7 ± 0.6 free thiols at high pO_2 in the presence of DPI) and PEG-catalase (39.4 ± 2.9 free thiols at low pO_2 versus 38.4 ± 2.9 free thiols at high pO_2 in the presence of PEG-catalase) (Table 1). These results, in combination with those described above, establish a causal relationship between O_2-coupled oxidation of RyR1 Cys thiols and RyR1 activation and indicate that H_2O_2 production intrinsic to the SR is the basis of this pO_2-dependent regulation.

Nox2 is associated with transverse tubules of mammalian skeletal muscle (17). However, we saw no effect on ROS production or pO_2-regulated RyR1 activity of the Nox2 inhibitor aminoethyl-benzenesulfono-fluoride (Fig. S4*A*), and pO_2-coupled ROS production and RyR1 activation were unaltered in SR vesicles derived from knockout mice deficient in Nox2 (Fig. S4 *B* and *C*). Analysis of rat hind-limb skeletal muscle by quantitative real-time PCR (Fig. S5*A*) indicated that Nox2 and Nox4 and Duox1 and Duox2 were expressed at significant levels and that Nox4 was substantially the most abundantly expressed form [Nox5 apparently is not expressed in rodents (18)]. We detected Nox4 (see below) but not Duox1 or Duox2 in isolated SR vesicles

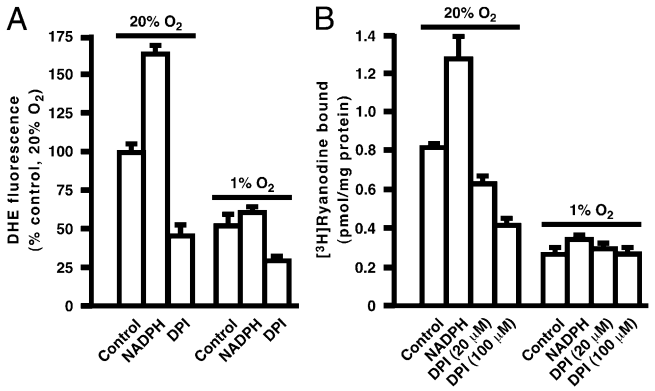

Fig. 2. Characterization of the ROS-generating activity of SR. In SR vesicles isolated from skeletal muscle of rabbit, (*A*) ROS production (DHE fluorescence) and (*B*) RyR1 activity ([^{3}H]-ryanodine binding) were enhanced at high versus low pO_2. At high pO_2, addition of NADPH (1 mM) enhanced production of O_2^-, and this enhancement was eliminated by DPI. ($n = 4$–6).

Table 1. pO_2- and H_2O_2-dependent loss of free thiols within RyR1

	21% O_2	1% O_2
Control	34.5 ± 2.4	39.9 ± 2.8
PEG-catalase	38.4 ± 2.0	39.4 ± 2.9
DPI	38.7 ± 0.6	39.6 ± 1.2

A small set of Cys thiols within RyR1 is oxidized at high versus low pO_2 as determined by thiol labeling of SR vesicles (numbers represent free thiols per RyR1 monomer), and the loss of thiols is blocked by removing H_2O_2 with membrane-permeable PEG-catalase or by treatment with the Nox inhibitor DPI.

by Western blotting. Nox4 activity does not require cytosolic subunits, and heterologously expressed Nox4 is constitutively active (19–21), consistent with regulation of ROS production by O_2 (substrate) level.

Analysis by Western blotting following subcellular fractionation of rat hind-limb muscle showed that Nox4 and RyR1 colocalize within the junctional SR (Fig. 3 *A* and *B*). Fluorescence immunohistochemistry of sections from rat hind-limb extensor muscle directly demonstrated colocalization of Nox4 and RyR1 (Fig. S5*B*), and RyR1 and Nox4 coimmunoprecipitated from solubilized SR vesicles (Fig. 3*C*).

We used knockdown with siRNA to assess the role of Nox4 using C2C12 cells, a skeletal muscle-derived cell line that provides a well-accepted model system. C2C12 cells were largely differentiated from myoblasts to multinucleated myotubes by 7 d in culture, and in differentiated C2C12 cells (9 d in culture) Nox4 was the most abundantly expressed form of Nox as assessed by PCR (Fig. S6*A*). Expression of Nox4 and RyR1 increased together as myotubes differentiated (Fig. S6*B*), and both Nox4 and RyR were most abundant in a microsomal (100,000 × *g*) fraction following subcellular fractionation of differentiated cells (Fig. S6*C*).

In the microsomal fraction derived from differentiated C2C12 cells, RyR activity was greater at high pO_2 than at low pO_2 (Fig. 4). Activity was enhanced at both low and high pO_2 by NADPH, and enhancement by NADPH was eliminated by DPI (Fig. 4).

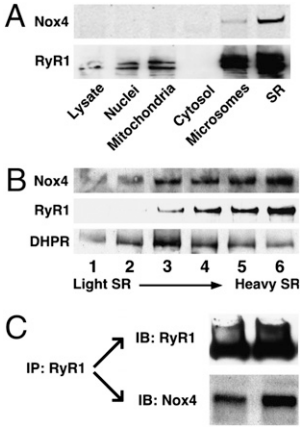

Fig. 3. Colocalization of Nox4 and RyR1 in skeletal muscle. (*A*) Subcellular fractionation of rat hind-limb muscle showed that Nox4 and RyR1 coenriched and were most abundant in the SR-enriched fraction isolated from the microsomal fraction by densit- gradient centrifugation. (*B*) Samples taken progressively from the top to the bottom of the SR-enriched gradient segment, which are progressively enriched in junctional SR (heavy SR) (45, 51), were increasingly enriched in both RyR1 and Nox4, whereas the dihydropyridine receptor/Ca^{2+} channel (DHPR), a constituent of transverse tubule membranes, exhibited a disparate pattern of enrichment. (*C*) Nox4 coimmunoprecipitates with RyR1 from solubilized SR vesicles; results of two separate experiments are shown.

Treatment of C2C12 cells with an siRNA specific for Nox4 (but not with scrambled, control siRNA) knocked down most Nox4 expression through at least 11 d in culture, without affecting RyR1 expression (Fig. S6*B*). Nox4 knockdown both eliminated the enhancement of RyR1 activity by NADPH at high pO_2 and reduced basal activity to levels indistinguishable from those observed in the presence of DPI (Fig. 4). Knockdown of Nox4 also eliminated the enhancement of RyR1 activity by NADPH at low pO_2 (Fig. 4). Similarly, ROS production by the microsomal fraction was greater at high pO_2 than at low pO_2, as assessed by DHE fluorescence, and DPI eliminated this difference (Fig. S6*D*. Nox4 knockdown also eliminated the difference in ROS production at high versus low pO_2, and ROS production at high pO_2 was indistinguishable from that seen in the presence of DPI (Fig. S6*D*). Finally, we verified with the fluorescent reporter 2′,7′-dichlorofluorescin (22) that the production of H_2O_2 by C2C12 microsomes was enhanced at high versus low pO_2 and by addition of NADPH (Fig. S6*E*). Following Nox4 knockdown, basal production of H_2O_2 at high pO_2 was suppressed, and the enhanced production at high versus low pO_2 following addition of NADPH was eliminated (Fig. S6*E*). These results were replicated with a second, nonoverlapping Nox4 siRNA (Fig. S7).Taken together, these results demonstrate that, although there clearly is more than one source of ROS in C2C12 microsomes, Nox4 accounts for NADPH-dependent ROS production and is the necessary and sufficient source of pO_2-coupled ROS production that regulates RyR1 activity.

We next explored the role of Nox4 in regulating stimulus-induced Ca^{2+} flux. In primary skeletal muscle myocytes derived from mouse flexor digitorum brevis, the amplitudes of Ca^{2+} transients induced by electrical depolarization (23), known to reflect RyR1 activation, were greater at 20% O_2 than at 1% O_2, and this difference was largely eliminated by treatment with PEG-catalase (Fig. 5*A* and Fig. S8*A*). In differentiated C2C12 cells, depolarization with KCl (50 mM) resulted in rapid increases in cytoplasmic Ca^{2+} levels (Fig. 5 *B* and *C* and Fig. S8*B*) that were eliminated by preincubation with ryanodine (Fig. 5*C*) and which therefore could be ascribed to RyR activation. Depolarization-induced Ca^{2+} release through RyR was greater at high versus low

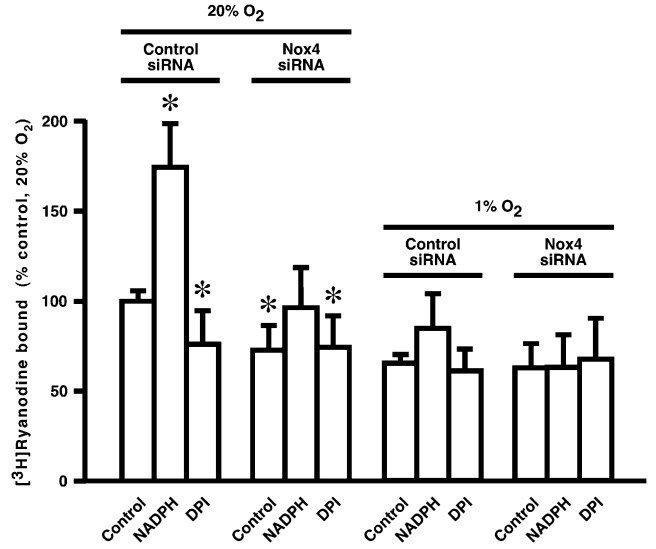

Fig. 4. ROS generated by Nox4 mediate pO_2-dependent regulation of RyR1 in C2C12 cells. RyR activity in the microsomal fraction from differentiated C2C12 cells (assessed by [^{3}H]-ryanodine binding) is enhanced at high versus low pO_2 and by the addition of NADPH (1 mM), and enhancement is abrogated by DPI (20 μM) and by siRNA-mediated knockdown of Nox4. For samples at 20% O_2, asterisks indicate significant difference versus control (*$P < 0.05$ re control at 20% O_2; n = 4–6).

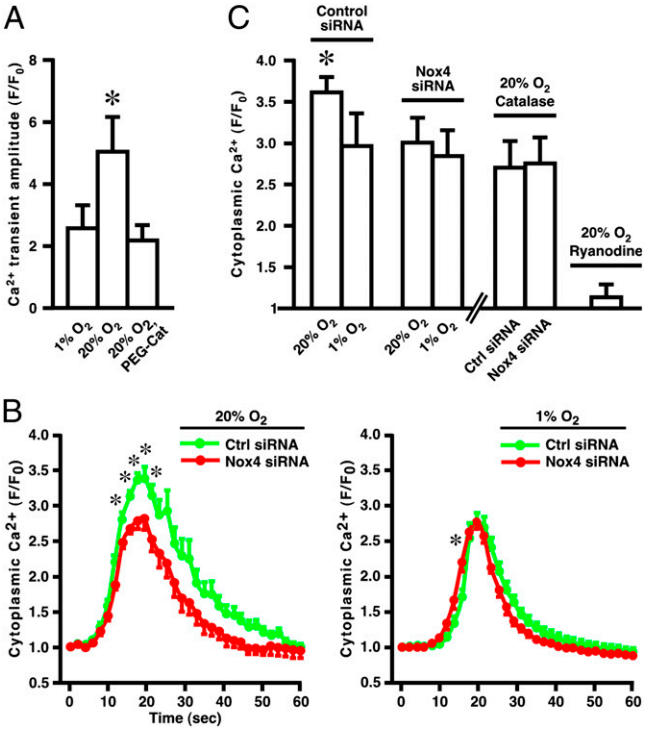

Fig. 5. Nox4 regulates stimulus-induced Ca^{2+} release through RyR1. (*A*) In primary skeletal muscle myocytes, electrically induced Ca^{2+} transients are greater at high than at low pO_2, and this difference is largely eliminated by PEG-catalase (n = 3–4; asterisk indicates $P < 0.05$). (*B*) In C2C12 cells, maximal cytoplasmic Ca^{2+} levels following depolarization by KCl (50 mM) are greater at high than at low pO_2, and this difference is eliminated by Nox4 knockdown with Nox4-specific siRNA. Nox4 knockdown does not affect Ca^{2+} levels at low pO_2 or the time to peak amplitude at high pO_2. Each data point was obtained by integrating fluorescence emission over three to five entire myofibers within a single microscopic field of view during a single experiment (myofibers were depolarized only once); n = 6–9. Asterisks indicate significant differences ($P < 0.05$). (*C*) For each condition, maximal depolarization-induced Fluo 3 fluorescence was measured by integrating within 12 subfields distributed within three to five fibers, in each of six to nine experiments. As indicated by an asterisk, ANOVA indicated a significant difference ($P \leq 0.016$) between the magnitude of Ca^{2+} release at high pO_2 in control siRNA-treated samples and all other conditions; there were no significant differences ($P \geq 0.465$) between any other pair of conditions (excluding the effects of ryanodine). Note that ryanodine eliminated K^+-induced Ca^{2+} release (n = 3), which therefore may be ascribed to RyR activity, and that elimination of H_2O_2 with PEG-catalase also eliminated the enhancement of Ca^{2+} release at high pO_2 (n = 5).

pO_2, and this difference was eliminated by Nox4 knockdown (Fig. 5 *B* and *C*). Ca^{2+} release at low pO_2 was not affected by Nox4 knockdown (Fig. 5 *B* and *C*). In addition, we verified that the effects of pO_2 on KCl-induced Ca^{2+} release through RyR1 in C2C12 cells were mediated by H_2O_2: the enhancement of Ca^{2+} release at high pO_2 was eliminated by PEG-catalase (Fig. 5*C*). Thus, Nox4 mediates regulation by O_2-derived H_2O_2 of stimulus-induced Ca^{2+} release through RyR1.

We then examined in bioassays the effects of pO_2 on contractility of isolated, intact mouse extensor digitorum longus (EDL), a predominantly fast-twitch hind-limb muscle. We reported previously that incubation of EDL at 1% O_2 and at 20% O_2 results in muscle core pO_2 of about 3.5 mm Hg and 37 mm Hg, respectively (2), levels that broadly recapitulate the pO_2 gradient in skeletal muscle across the continuum of resting muscle to moderate exercise (4–7). The curve describing the relationship between tetanic stimulation frequency and evoked force (force-frequency curve) was progressively left-shifted at 5% O_2 and 20% O_2 versus 1% O_2 (Fig. 6*A*). En-

hanced contractility at higher pO_2 was reduced by incubation with PEG-catalase (Fig. 6*B*). Thus, excitation–contraction coupling in skeletal muscle is pO_2 sensitive, and H_2O_2 conveys at least a significant part of the pO_2-coupled regulatory signal.

To verify a role for Nox4 in pO_2-coupled regulation of contractility, we used local administration of an adeno-associated viral vector, AAV6, to express Nox4-directed shRNA in intact EDL muscle, followed after 4 wk by bioassay. As used (*Materials and Methods*), percutaneous hind-limb injection of vector resulted in variable degrees of Nox4 knockdown in EDL as assessed by Western blotting (Fig. S9), but the extent of Nox4 knockdown was correlated strongly with the observed decrease in tetanic force generation (Fig. 6*C*), and knockdown decreased force production to a greater extent at 20% O_2 than at 1% O_2 (Fig. 6*C*). For EDL muscles in which Nox4 knockdown was ≥60%, tetanic force production at 20% O_2 was decreased by about 70% (Fig. 6*D*).

Discussion

Our results may provide insights into the molecular mechanisms of O_2 sensing and O_2-based signaling in mammalian cells and into the nature and functional significance of redox-based regulation of skeletal muscle function. In particular, although a potential role for Noxs in O_2 sensing has long been considered (24, 25), and a role for Nox4 has received support from in vitro evidence derived from heterologous expression (26) and recently from analysis of hypoxic pulmonary vasoconstriction (27), no molecular mechanisms have been adduced. In addition, although oxidation of Cys thiols within RyR1 is associated with multiple disease states (28–30), a physiological role for Cys thiol modification by ROS has not been suggested heretofore, and in situ sources of ROS that might act upon RyR1 under physiological conditions have not been identified. Here we demonstrate a role for H_2O_2 that is derived from SR-localized Nox4 in O_2-coupled regulation of RyR1 under physiologically relevant conditions.

We reported previously that RyR1 is activated by oxidation of a small set of Cys thiols at higher pO_2, and that oxidation also prevents S-nitrosylation of a separate Cys thiol that activates RyR1 at low pO_2 (1, 2). However, the molecular mechanism responsible for oxidation of these allosteric thiols and thus for pO_2-dependent regulation of RyR1 activity remained unknown. We now show that this mechanism is provided by SR-resident Nox4. We also reported previously that RyR2, the principal form of RyR in the SR of cardiac striated muscle, is activated at high versus low pO_2 in association with loss of a small set of Cys thiols (31). The present results suggest that H_2O_2 produced by Nox4 likely serves to regulate RyR2 in cardiac muscle as well. The relationship between RyR1 Cys residues modified in a Nox4- and pO_2-dependent fashion and those identified as redox sensitive in previous studies (32, 33) remains to be determined. In situ, muscle activation is associated with a decline in pO_2 (and therefore in Nox4-derived ROS) and also with enhanced NO production (34). The present results thus suggest that the generation of H_2O_2 by Nox4 provides a molecular basis for the coordinated actions of NO and O_2 on RyR1 that subserve redox regulation of skeletal muscle contractility over the physiological range of pO_2.

Specialized oxygen-sensing cells apparently share a common approach to transducing alterations in pO_2: Regulation of K^+-

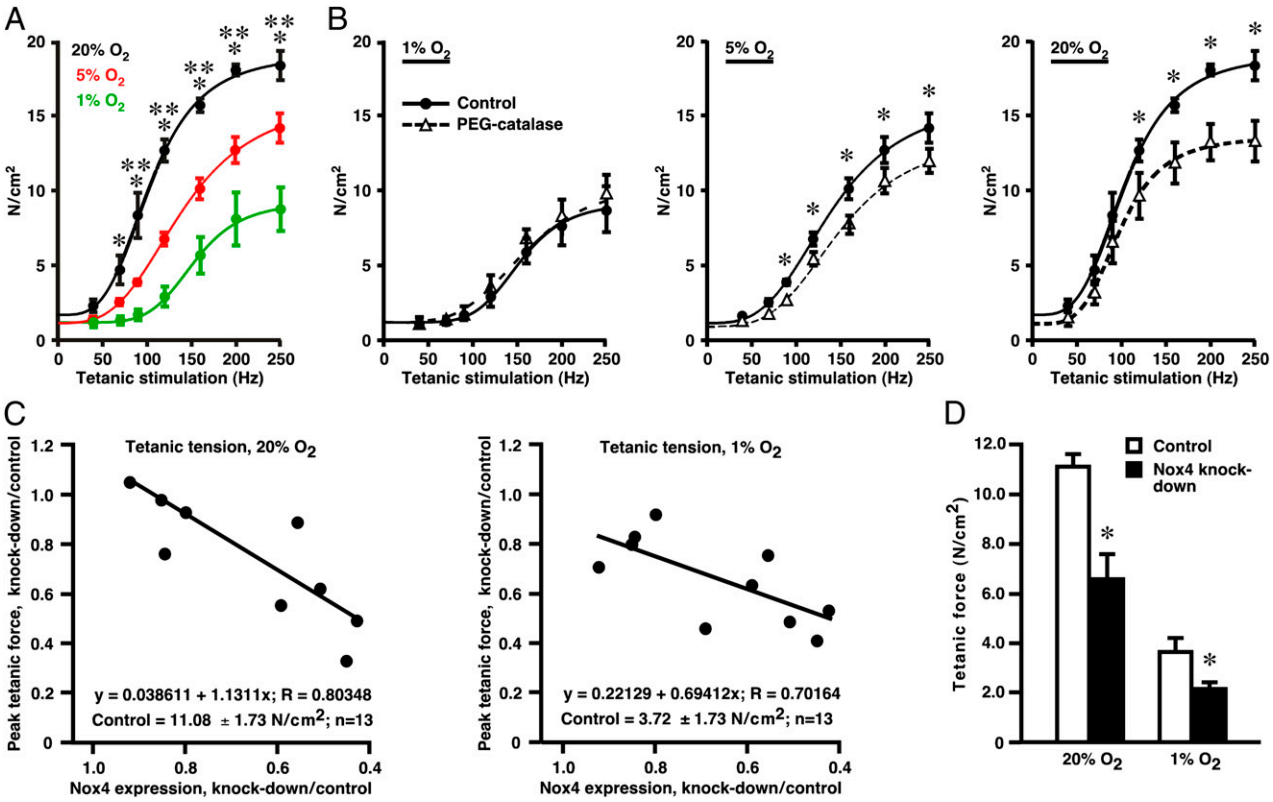

Fig. 6. pO_2-dependent regulation of muscle contractility by endogenous ROS. (*A*) Contractile force evoked by tetanic stimulation (40–250 Hz) of isolated, intact mouse EDL muscles at 1% O_2, 5% O_2, or 20% O_2 and (*B*) the effects of PEG-catalase (500 U/mL). (*A*) Plots of force generation versus stimulus frequency reveal a leftward (facilitatory) shift as a function of increasing pO_2. $^*P < 0.05$, 1% and 20% O_2; $^{**}P < 0.05$, 1% versus 5% O_2 (two-way ANOVA; $n = 3$–4). (*B*) Force generation is reduced by PEG-catalase at 20% and at 5% O_2 but not at 1% O_2. $^*P < 0.05$, control values versus values in the presence of PEG-catalase (two-way ANOVA; $n = 3$–4). (*C*) Contractile force induced by maximal tetanic stimulation (250 Hz) of isolated, intact mouse EDL muscle decreases in proportion to the degree of shRNA-mediated Nox4 knockdown. (*D*) A histogram illustrates the decrease in tetanic force generation for muscles in which knockdown of Nox4 was ≥60% ($^*P < 0.05$ re control; $n = 5$).

channel activity (hypoxia-coupled inhibition) results in modulation (enhancement) of Ca^{2+} influx through voltage-gated Ca^{2+} channels (35–37). Consistent with a potential role for Nox(s) (24, 25), the reported effects on K^+ channel activity and hypoxic signaling of exogenous thiol oxidants (enhancement) and reductants (suppression) generally have been consistent with coupling between endogenous ROS production and channel activity (38). However, the evidence bearing on a role for Nox(s) in O_2 sensing is contradictory (10, 11, 35, 37), and in general studies in knockout mice have not supported a role for Nox2 (39–41). Our present and previous (1) findings indicate that, in the case of RyR1, O_2-based signaling is mediated by reversible channel oxidation/reduction coupled to H_2O_2 production by Nox4 that results in channel activation/deactivation. Thus, in at least some other cell types, hypoxia-coupled decreases in K^+ channel activity may represent a disfacilitation of channel activation otherwise maintained by pO2- and Nox4-coupled channel oxidation.

Aberrant oxidation of Cys thiols within RyR1 and RyR2, which may be linked to dysregulated S-nitrosylation, contributes to Ca^{2+} leak through RyR1 in muscle pathophysiologies including extreme exercise-induced fatigue, central core disease, malignant hypothermia, and muscular dystrophy (28–30) and in the case of RyR2 may contribute to aberrant cardiac contractility (30, 42–44). All these disorders are characterized by tissue O_2 deficits and/or aberrant O_2 processing, as are a wide range of additional diseases, including sickle cell disease, sepsis, diabetes, and heart failure, in which myopathy is an established but poorly understood feature. It may be worthwhile to examine the role of Nox4 in muscle disorders and more generally in pathophysiological conditions characterized by disordered tissue oxygenation.

Materials and Methods

Subcellular Fractionation of Skeletal Muscle, Preparation of SR Vesicles, and Purification of RyR1. SR vesicles were prepared essentially as described (1, 45). Briefly, hind-limb muscle from rabbit or mouse was homogenized in buffer containing 20 mM Hepes (pH 7.4), 2 mM EDTA, 0.2 mM EGTA, 0.3 M sucrose, and protease inhibitors (100 nM aprotinin, 20 μM leupeptin, 1 μM pepstatin, 0.2 mM phenylmethylsulfonyl fluoride, 1 mM benzamidine). Homogenates then were subjected to differential centrifugation: 100 × *g* for 10 min (to remove unbroken cells and debris); 1,000 × *g* for 10 min (to pellet nuclei); 10,000 × *g* for 20 min (to pellet mitochondria); and 100,000 × *g* for 1 h (to generate a membrane-enriched microsomal pellet and cytosol-enriched supernatant).

To isolate SR vesicles, the pellet generated at 100,000 × *g* (the membrane fraction) was resuspended and fractionated on a continuous 20–45% sucrose gradient (without KCl) by centrifugation at 100,000 × *g* for 14 h. Heavy and light SR vesicle fractions were eluted separately and, after collection by centrifugation at 120,000 × *g*, were resuspended, aliquoted, and stored in liquid nitrogen. RyR1 was purified from SR vesicles solubilized with CHAPS by sucrose density gradient centrifugation as described (1, 46). Protein concentrations were determined with a bicinchoninic acid-based assay.

Assay of RyR1 Activity by ^{3}H-Ryanodine Binding. RyR1 activity was assayed essentially as described (1). Isolated SR vesicles or microsomal membranes were incubated overnight with 5 nM [^{3}H]-ryanodine at room temperature in medium containing 20 mM imidazole/125 mM KCl (pH 7.0), 0.3 mM Pefabloc (Roche), 30 μM leupeptin, and 10 μM free Ca^{2+}. The medium was bubbled continuously with a gas mixture containing a fixed concentration of O_2 as specified, 5% CO_2, remainder N_2. Nonspecific binding was determined using a 1,000-fold excess of unlabeled ryanodine. After incubation, samples were diluted with 20 vol H_2O at 4 °C and placed on Whatman GF/B filters soaked with 2% (wt/wt) polyethyleneimine. Filters were washed three times by vacuum with 5 mL buffer per wash (1 mM Pipes, 0.1 M KCl, pH 7.0), and the radioactivity remaining on the filters was quantified by liquid scintillation counting.

Quantification of Protein Sulfhydryls (Free Thiols). The free thiol content of RyR1 was quantified by monobromobimane fluorescence (MBB; Molecular Probes) (47). As described (1), MBB labeling was carried out in SR vesicle preparations in the presence of 10 μM Ca^{2+}.

Assay of ROS Production by DHE Conversion. Isolated SR vesicles or C2C12 microsomal fractions were incubated with 10 μM DHE (Molecular Probes) (8) for 20 min at room temperature and controlled pO_2 (glove box) in 200 μL buffer per sample [20 mM imidazole/125 mM KCl (pH 7.0), 10 μM Ca^{2+}] in 96-well microplates (0.4 μg protein/μL), and plates were read with a fluorescence microplate reader (excitation 510 nm; emission 590 nm). When used, DPI, NADPH, VAS2870, or PEG-catalase was added 30 min before DHE.

Assay of H_2O_2 with 2′,7′-Dichlorofluorescein. H_2O_2 production was measured essentially as described (22). Isolated C2C12 microsomes were incubated with 10 μM 5-(and-6)-chloromethyl-2′,7′-dichlorodihydrofluorescein diacetate, acetyl ester (CM-H_2DCFDA; Molecular Probes) for 20 min at room temperature and controlled pO_2 (glove box) in 200 μL buffer per sample [20 mM imidazole/125 mM KCl (pH 7.0), 10 μM Ca^{2+}, and 100 mg/mL HRP, ± 1 mM NADPH) in 96-well microplates (0.3 μg protein/μL), and plates were read with a fluorescence microplate reader (excitation 485 nm; emission 520 nm).

Nox4 Expression. RNA isolation, quantitative PCR, immunoprecipitation, Western blot analysis, and immunohistochemistry were carried out as described in *SI Materials and Methods*.

Analysis of Nox4/RyR1 in C2C12 Cells. Culture of C2C12 cells, siRNA-mediated knockdown of Nox4, and assay of intracellular Ca^{2+} release with Fluo 3-AM were carried out as described in *SI Materials and Methods*.

Assay of Intracellular Ca^{2+} Release: Primary Myocytes. Single fibers were isolated from the flexor digitorum brevis hind-limb muscle of mice essentially as described (48, 49). Muscle bundles were dissected and incubated in Tyrode's solution containing 2 mg/mL collagenase (type II; Worthington) for 3 h at 37 °C and then were transferred to DMEM supplemented with BSA as well as 50 U/mL penicillin and 50 mg/mL streptomycin. Individual myofibers were generated by trituration, collected by centrifugation at 1,000 × *g* for 3 min, and resuspended in DMEM. Myofibers then were incubated at 37 °C under 5% CO_2, remainder room air, for 2–3 d.

To obtain measurements of Ca^{2+} transients, myofibers were loaded with Fluo 3-AM (5 μM) for 45 min with or without PEG-catalase (10 units/mL). Myofibers were suspended in Tyrode's solution and placed in a sealed chamber designed for field stimulation (RC-21BRFS; Warner Instruments) that was superfused with a continuous linear flow of Tyrode's solution externally sparged with room air or 1% O_2/5% CO_2 (remainder nitrogen). Myofibers were visualized using an inverted Axiovert microscope (Zeiss) and simulated at 1 Hz (1-ms duration; ~40–50 V). Ca^{2+} signals (Fluo 3-AM fluorescence emission) were recorded with a CCD camera system (PentaMAX; Princeton Instruments). Ca^{2+} transient amplitude was measured as the difference between peak systolic and baseline diastolic levels and was normalized to baseline fluorescence (F/F_o).

Intact Muscle Bioassay. Muscle bioassays were carried out essentially as described (2). EDL muscles were obtained from male mice at 8–10 wk of age. Each assay comprised both EDL muscles from two mice. Individual muscles were suspended from proximal and distal tendons, in series with force transducers, in organ baths containing Kreb's solution (pH 7.4) at 37 °C and were continuously gassed with 20% O_2 and 5% CO_2 (remainder NO_2). After equilibration (see below), each muscle was adjusted to the length at which isometric twitch-force generation was maximal (optimal muscle length, L_o) and subjected to a single train of tetanic stimulation (160 Hz) to assess force generation qualitatively. Stimulation consisted of trains of pulses (train duration 75 ms; individual pulse duration, 2 ms; pulse frequency, 40–250 Hz; pulse amplitude, 60 V, which is about 75% of the amplitude that elicited maximal twitch force) delivered through platinum electrodes (7.0 mm wide) placed parallel to the long axis of the muscle. At least 2 min elapsed between trains of tetanic stimuli. For each muscle, L_o was measured after testing, the muscle was weighed wet, and the effective cross-sectional area was calculated by approximating the muscle as a cylinder of length L_o and a density of 1.06 $g \cdot cm^{-3}$ (2). Force production was normalized with respect to EDL cross-sectional area (N/cm^2).

After the determination of L_o, muscles were allowed to equilibrate for ~10 min at 20% O_2, after which pO_2 was maintained at 20% O_2 or was switched to 1% O_2 or 5% O_2. Force production was assessed 10 min or 90 min later. When used, PEG-catalase was added to the bath after the initial 10-min equilibration, and muscles were incubated for 90 min at 20% O_2, followed by 10-min exposure at 1% O_2, 5% O_2, or 20% O_2 before testing.

Nox4 Knockdown in Intact Muscle. Construction and administration of the Nox4 shRNA-AAV vector were as described in ref. 50 and in *SI Materials and Methods*.

ACKNOWLEDGMENTS. We thank Dr. D. Lambeth for supplying antibody to Nox4 and Dr. H. Schmidt for providing VAS2870. This work was supported by National Institutes of Health RO1 Grants HL0591130 and AR018687.

1. Eu JP, Sun J, Xu L, Stamler JS, Meissner G (2000) The skeletal muscle calcium release channel: Coupled O_2 sensor and NO signaling functions. *Cell* 102:499–509.
2. Eu JP, et al. (2003) Concerted regulation of skeletal muscle contractility by oxygen tension and endogenous nitric oxide. *Proc Natl Acad Sci USA* 100:15229–15234.
3. Sun J, Xin C, Eu JP, Stamler JS, Meissner G (2001) Cysteine-3635 is responsible for skeletal muscle ryanodine receptor modulation by NO. *Proc Natl Acad Sci USA* 98: 11158–11162.
4. Gorczynski RJ, Duling BR (1978) Role of oxygen in arteriolar functional vasodilation in hamster striated muscle. *Am J Physiol* 235:H505–H515.
5. Molé PA, et al. (1999) Myoglobin desaturation with exercise intensity in human gastrocnemius muscle. *Am J Physiol* 277:R173–R180.
6. Richardson RS, Newcomer SC, Noyszewski EA (2001) Skeletal muscle intracellular $PO(_2)$ assessed by myoglobin desaturation: Response to graded exercise. *J Appl Physiol* 91: 2679–2685.
7. Richardson RS, et al. (2006) Human skeletal muscle intracellular oxygenation: The impact of ambient oxygen availability. *J Physiol* 571:415–424.
8. Tarpey MM, Fridovich I (2001) Methods of detection of vascular reactive species: Nitric oxide, superoxide, hydrogen peroxide, and peroxynitrite. *Circ Res* 89:224–236.
9. Weir EK, López-Barneo J, Buckler KJ, Archer SL (2005) Acute oxygen-sensing mechanisms. *N Engl J Med* 353:2042–2055.
10. Sommer N, et al. (2008) Regulation of hypoxic pulmonary vasoconstriction: Basic mechanisms. *Eur Respir J* 32:1639–1651.
11. Weissmann N, et al. (2006) Oxygen sensors in hypoxic pulmonary vasoconstriction. *Cardiovasc Res* 71:620–629.
12. Khan SA, et al. (2004) Neuronal nitric oxide synthase negatively regulates xanthine oxidoreductase inhibition of cardiac excitation-contraction coupling. *Proc Natl Acad Sci USA* 101:15944–15948.
13. Bedard K, Krause KH (2007) The NOX family of ROS-generating NADPH oxidases: Physiology and pathophysiology. *Physiol Rev* 87:245–313.
14. Lambeth JD, Kawahara T, Diebold B (2007) Regulation of Nox and Duox enzymatic activity and expression. *Free Radic Biol Med* 43:319–331.
15. Takac I, et al. (2011) The E-loop is involved in hydrogen peroxide formation by the NADPH oxidase Nox4. *J Biol Chem* 286:13304–13313.
16. Stielow C, et al. (2006) Novel Nox inhibitor of oxLDL-induced reactive oxygen species formation in human endothelial cells. *Biochem Biophys Res Commun* 344:200–205.
17. Hidalgo C, Sánchez G, Barrientos G, Aracena-Parks P (2006) A transverse tubule NADPH oxidase activity stimulates calcium release from isolated triads via ryanodine receptor type 1 S -glutathionylation. *J Biol Chem* 281:26473–26482.
18. Sumimoto H (2008) Structure, regulation and evolution of Nox-family NADPH oxidases that produce reactive oxygen species. *FEBS J* 275:3249–3277.
19. Ago T, et al. (2004) Nox4 as the major catalytic component of an endothelial NAD(P)H oxidase. *Circulation* 109:227–233.
20. Martyn KD, Frederick LM, von Loehneysen K, Dinauer MC, Knaus UG (2006) Functional analysis of Nox4 reveals unique characteristics compared to other NADPH oxidases. *Cell Signal* 18:69–82.
21. Serrander L, et al. (2007) NOX4 activity is determined by mRNA levels and reveals a unique pattern of ROS generation. *Biochem J* 406:105–114.
22. Black MJ, Brandt RB (1974) Spectrofluorometric analysis of hydrogen peroxide. *Anal Biochem* 58:246–254.
23. Liu Y, Carroll SL, Klein MG, Schneider MF (1997) Calcium transients and calcium homeostasis in adult mouse fast-twitch skeletal muscle fibers in culture. *Am J Physiol* 272:C1919–C1927.
24. Acker H (1989) PO_2 chemoreception in arterial chemoreceptors. *Annu Rev Physiol* 51: 835–844.
25. Acker H, Dufau E, Huber J, Sylvester D (1989) Indications to an NADPH oxidase as a possible pO_2 sensor in the rat carotid body. *FEBS Lett* 256:75–78.
26. Lee YM, et al. (2006) NOX4 as an oxygen sensor to regulate TASK-1 activity. *Cell Signal* 18:499–507.
27. Ahmad M, Kelly MR, Zhao X, Kandhi S, Wolin MS (2010) Roles for Nox4 in the contractile response of bovine pulmonary arteries to hypoxia. *Am J Physiol Heart Circ Physiol* 298:H1879–H1888.
28. Durham WJ, et al. (2008) RyR1 S-nitrosylation underlies environmental heat stroke and sudden death in Y522S RyR1 knockin mice. *Cell* 133:53–65.
29. Bellinger AM, et al. (2008) Remodeling of ryanodine receptor complex causes "leaky" channels: A molecular mechanism for decreased exercise capacity. *Proc Natl Acad Sci USA* 105:2198–2202.
30. Bellinger AM, et al. (2009) Hypernitrosylated ryanodine receptor calcium release channels are leaky in dystrophic muscle. *Nat Med* 15:325–330.
31. Sun J, et al. (2008) Regulation of the cardiac muscle ryanodine receptor by $O(_2)$ tension and S-nitrosoglutathione. *Biochemistry* 47:13985–13990.
32. Voss AA, Lango J, Ernst-Russell M, Morin D, Pessah IN (2004) Identification of hyperreactive cysteines within ryanodine receptor type 1 by mass spectrometry. *J Biol Chem* 279:34514–34520.
33. Aracena-Parks P, et al. (2006) Identification of cysteines involved in *S*-nitrosylation, *S*-glutathionylation, and oxidation to disulfides in ryanodine receptor type 1. *J Biol Chem* 281:40354–40368.
34. Stamler JS, Meissner G (2001) Physiology of nitric oxide in skeletal muscle. *Physiol Rev* 81:209–237.
35. Dinger B, et al. (2007) The role of NADPH oxidase in carotid body arterial chemoreceptors. *Respir Physiol Neurobiol* 157:45–54.
36. Buckler KJ (2007) TASK-like potassium channels and oxygen sensing in the carotid body. *Respir Physiol Neurobiol* 157:55–64.
37. Kemp PJ (2006) Detecting acute changes in oxygen: Will the real sensor please stand up? *Exp Physiol* 91:829–834.
38. Weir EK, Archer SL (2006) Counterpoint: Hypoxic pulmonary vasoconstriction is not mediated by increased production of reactive oxygen species. *J Appl Physiol* 101: 995–998, discussion 998.
39. Roy A, et al. (2000) Mice lacking in gp91 phox subunit of NAD(P)H oxidase showed glomus cell $[Ca(^{2+})](_i)$ and respiratory responses to hypoxia. *Brain Res* 872:188–193.
40. He L, et al. (2002) Characteristics of carotid body chemosensitivity in NADPH oxidase-deficient mice. *Am J Physiol Cell Physiol* 282:C27–C33.
41. Archer SL, et al. (1999) O_2 sensing is preserved in mice lacking the gp91 phox subunit of NADPH oxidase. *Proc Natl Acad Sci USA* 96:7944–7949.
42. Gonzalez DR, Beigi F, Treuer AV, Hare JM (2007) Deficient ryanodine receptor S-nitrosylation increases sarcoplasmic reticulum calcium leak and arrhythmogenesis in cardiomyocytes. *Proc Natl Acad Sci USA* 104:20612–20617.
43. Fauconnier J, et al. (2010) Leaky RyR2 trigger ventricular arrhythmias in Duchenne muscular dystrophy. *Proc Natl Acad Sci USA* 107:1559–1564.
44. Gonzalez DR, Treuer AV, Castellanos J, Dulce RA, Hare JM (2010) Impaired S-nitrosylation of the ryanodine receptor caused by xanthine oxidase activity contributes to calcium leak in heart failure. *J Biol Chem* 285:28938–28945.
45. Anderson K, Cohn AH, Meissner G (1994) High-affinity [^{3}H]PN200-110 and [^{3}H]ryanodine binding to rabbit and frog skeletal muscle. *Am J Physiol* 266:C462–C466.
46. Meissner G, Henderson JS (1987) Rapid calcium release from cardiac sarcoplasmic reticulum vesicles is dependent on Ca^{2+} and is modulated by Mg^{2+}, adenine nucleotide, and calmodulin. *J Biol Chem* 262:3065–3073.
47. Kosower NS, Kosower EM (1987) Thiol labeling with bromobimanes. *Methods Enzymol* 143:76–84.
48. Shefer G, Yablonka-Reuveni Z (2005) Isolation and culture of skeletal muscle myofibers as a means to analyze satellite cells. *Methods Mol Biol* 290:281–304.
49. Wozniak AC, et al. (2003) C-Met expression and mechanical activation of satellite cells on cultured muscle fibers. *J Histochem Cytochem* 51:1437–1445.
50. Grieger JC, Choi VW, Samulski RJ (2006) Production and characterization of adeno-associated viral vectors. *Nat Protoc* 1:1412–1428.
51. Lai FA, Erickson HP, Rousseau E, Liu QY, Meissner G (1988) Purification and reconstitution of the calcium release channel from skeletal muscle. *Nature* 331: 315–319.